Acta Cryst E CRYSTALLOGRAPHIC COMMUNICATIONS
ISSN 2056-9890

Crystal structure and optical spectroscopic analyses of (*E*)-3-(1*H*-indol-2-yl)-1-(4-nitrophenyl)prop-2-en-1-one hemihydrate

Muhamad Fikri Zaini,[a] Ibrahim Abdul Razak,[a] Wan Mohd Khairul[b] and Suhana Arshad[a]*

[a]X-ray Crystallography Unit, School of Physics, Universiti Sains Malaysia, 11800 USM, Penang, Malaysia, and [b]School of Fundamental Science, Universiti Malaysia Terengganu, 21030, Kuala Terengganu, Terengganu, Malaysia. *Correspondence e-mail: suhanaarshad@usm.my

Received 17 September 2018
Accepted 11 October 2018

Edited by A. J. Lough, University of Toronto, Canada

Keywords: chalcone; crystal structure; DFT; UV–vis; HOMO–LUMO; Hirshfeld surface.

CCDC reference: 1846181

Supporting information: this article has supporting information at journals.iucr.org/e

The asymmetric unit of the title compound, $2C_{17}H_{12}N_2O_3\cdot H_2O$ comprises two molecules of (*E*)-3-(1*H*-indol-2-yl)-1-(4-nitrophenyl)prop-2-en-1-one and a water molecule. The main molecule adopts an *s-cis* configuration with respect to the C=O and C=C bonds. The dihedral angle between the indole ring system and the nitro-substituted benzene ring is 37.64 (16)°. In the crystal, molecules are linked by O—H···O and N—H···O hydrogen bonds, forming chains along [010]. In addition, weak C—H···O, C—H···π and π–π interactions further link the structure into a three-dimensional network. The optimized structure was generated theoretically *via* a density functional theory (DFT) approach at the B3LYP/6–311 G++(d,p) basis level and the HOMO–LUMO behaviour was elucidated to determine the energy gap. The obtained values of 2.70 eV (experimental) and 2.80 eV (DFT) are desirable for optoelectronic applications. The intermolecular interactions were quantified and analysed using Hirshfeld surface analysis.

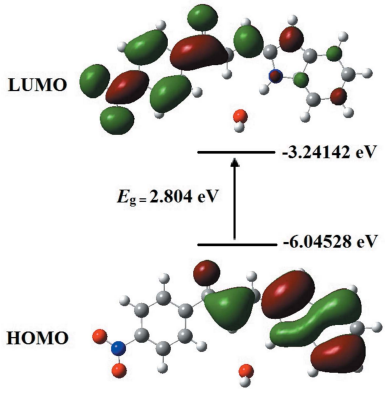

1. Chemical context

Chalcone compounds consist of open-chain flavanoids in which two aromatic rings are joined by a three carbon α,β-unsaturated carbonyl system (Thanigaimani *et al.*, 2015). The design of the chalcone system such as donor–π–acceptor (*D*–π–*A*) plays a significant role in intramolecular charge–transfer transitions (ICT) in which optical excitation leads to the movement of charge from the donor group to the acceptor group. In addition, the chalcone bridge consists of two different double bonds, C=C and C=O, which contribute to the conjugation of charge transfer, leading to their excellent structural and spectroscopic properties (de Toledo *et al.*, 2018). Furthermore, the non-linear optical (NLO) properties of chalcone molecules originate mainly from a strong donor–acceptor intramolecular interaction and delocalization of the π-electrons (Prabhu *et al.*, 2015). Many researchers are currently investigating the nitro (NO_2) group as an acceptor group because the decrease of the resonance effect leads to substantial changes in π-electron delocalization in the ring (Dobrowolski *et al.*, 2009). In this work, the title chalcone compound was successfully synthesized and its crystal structure is reported herein.

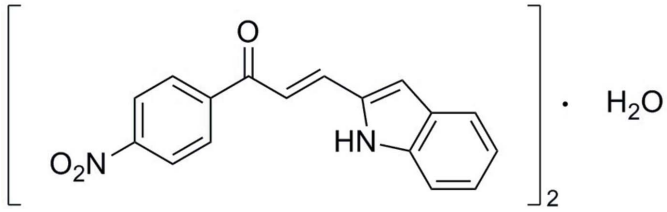

2. Structural commentary

The molecular structure of the title compound is shown in Fig. 1*a*. The structure was optimized with the *Gaussian09W* software package using the DFT method at the B3LYP/6-311G++(d,p) level, providing information about the geometry of the molecule. The optimized structure is shown in Fig. 1*b*. The geometrical parameters are mostly within normal ranges, the slight deviations from the experimental values are due to the fact that the optimization is performed in isolated conditions, whereas the crystal environment and hydrogen-bonding interactions affect the results of the X-ray structure (Zainuri *et al.*, 2017).

In the title compound, the enone group (O1/C9–C11) adopts an *s-cis* configuration with respect to the C11═O1 [1.209 (4) Å] and C9═C10 [1.310 (5) Å] bonds. The compound is twisted about the C10—C11 bond with C9—C10—C11—O1 torsion angle of −21.9 (6)°. The corresponding torsion angle obtained from the DFT study is 0.08°. In addition, the molecule is twisted about the C11—C12 bond with an O1—C11—C12—C13 torsion angle of 167.7 (4)° (calculated value 179.4°). The differences between the experimental and calculated values show that the intermolecular hydrogen bond involving the water molecule does not affect the planarity of the compound. A previous study (Zheng *et al.*, 2016) reported that the intermolecular hydrogen bond present in the optimized structure stabilizes both the main molecule and the water molecule, which is why we claim that the hydrogen bond does affect the planar conformation in our optimized structure. In the experimental structure, a weak intermolecular hydrogen bond involving an O atom of the nitro group (Table 1) may be responsible for the distortion from planarity of the molecule. Furthermore, the twisted nature of this part of the molecule might also be expected because of the steric effects between the carbonyl group and the nitro-substituted benzene ring (Kozlowski *et al.*, 2007).

The overall conformation of the molecule can be described by the dihedral angle formed by the indole ring system (N1/C1–C8) and the nitro-substituted benzene (C12–C17) ring with a value of 37.64 (16)° (Fig. 1*c*). The enone group (O1/C9–C11) with maximum deviation of 0.082 (3) Å at C11 forms dihedral angles of 21.5 (2) and 16.3 (2)° with the indole ring system and the nitro-substituted benzene ring, respectively.

Table 1
Hydrogen-bond geometry (Å, °).

*Cg*1 is the centroid of the N1/C1/C6–C8 ring.

D—H···*A*	*D*—H	H···*A*	*D*···*A*	*D*—H···*A*
O1*W*—H1*OW*···O1^{i}	0.88 (4)	1.86 (4)	2.723 (4)	171 (4)
N1—H1*A*···O1*W*	0.87 (3)	2.06 (3)	2.923 (4)	170 (3)
C4—H4*A*···O2^{ii}	0.93	2.60	3.405 (6)	146
C9—H9*A*···*Cg*1^{iii}	0.93	2.87	3.518 (4)	127

Symmetry codes: (i) $-x+2, y-1, -z+\frac{1}{2}$; (ii) $x-\frac{1}{2}, -y+\frac{1}{2}, z-\frac{1}{2}$; (iii) $-x+\frac{3}{2}, y+\frac{1}{2}, -z+\frac{1}{2}$.

3. Supramolecular features

In the crystal, four symmetry-related molecules are connected to each other *via* O—H···O and N—H···O hydrogen bonds involving the solvent water molecule. The water molecule is connected to the carbonyl group and indole ring system by intermolecular O1*W*—H1*OW*···O1^{i} and N1—H1*A*···O1*W* hydrogen bonds (Table 1), forming chains extending along the *b*-axis direction (Fig. 2). In addition, weak C4—H4*A*···O2^{ii} interactions (Table 1) link these chains into sheets parallel to

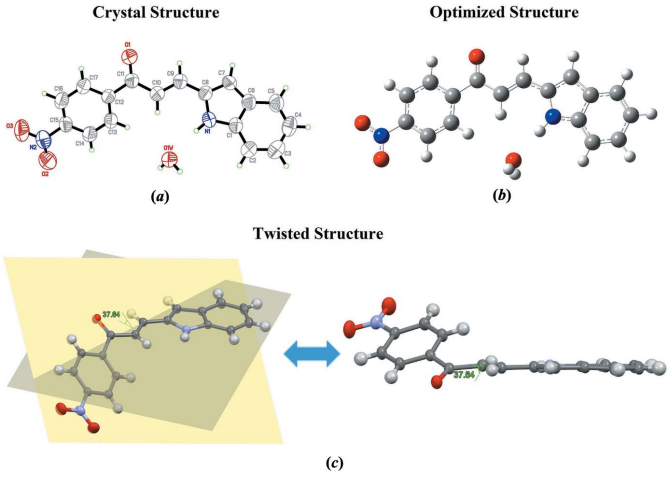

Figure 1
(*a*) The molecular structure of the title compound showing 50% probability ellipsoids, (*b*) the optimized molecular structure and (*c*) a representation of the molecule showing the dihedral angle between the two chosen planes.

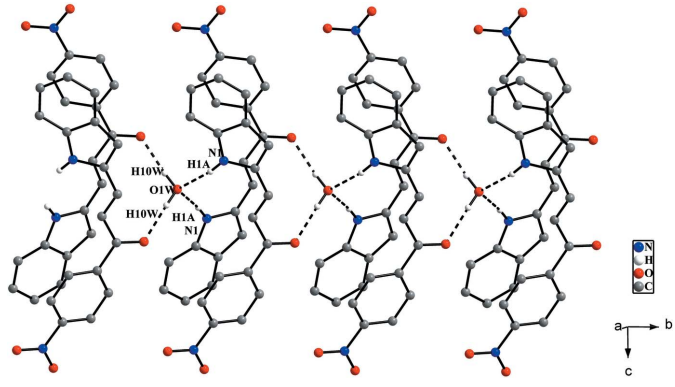

Figure 2
The crystal packing of the title compound along the *b* axis showing the O—H···O and N—H···O hydrogen bonds as dotted lines.

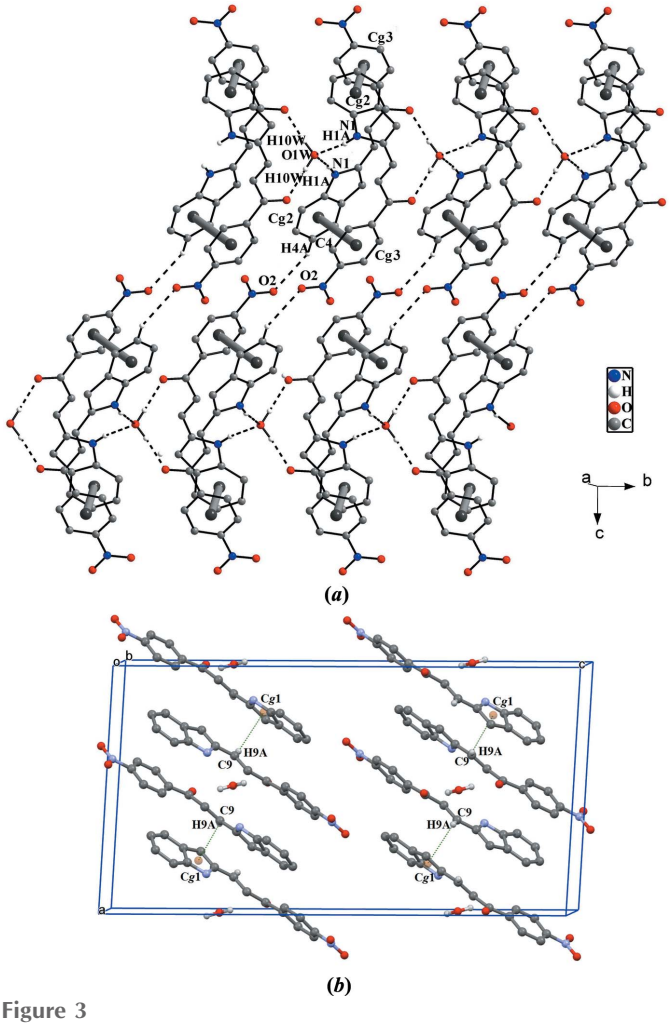

Figure 3
(*a*) A view of the crystal packing showing two of the chains linked by C—H···O interactions extending along *c*-axis direction. The π–π stacking interactions shown by grey lines further stabilize the crystal structure. (*b*) C—H···π interactions in the title compound. H atoms not involved in hydrogen-bonding interactions have been omitted for clarity.

the *bc* plane (Fig. 3*a*). Furthermore, C9—H9*A*···*Cg*1 interactions (*Cg*1 is the centroid of the N1/C1/C6–C8 ring; Table 1, Fig. 3*b*) are observed along the *a*-axis direction, completing the three-dimensional structure. Two of the anti-parallel molecules are linked by π–π stacking interactions (Fig. 3*a*) involving the centroids (*Cg*2 and *Cg*3) of the C1–C6 and C12–C17 rings with a centroid–centroid distance *Cg*2···*Cg*3 (2-*x*, *y*, 1/2 - *z*) of 3.534 (3) Å. These π–π interactions further stabilize the crystal structure.

4. Hirshfeld surface analysis

Analysis of the Hirshfeld surfaces provides a three-dimensional representation of intermolecular interactions. The Hirshfeld surfaces and related two-dimensional fingerprint (FP) plots were generated with *CrystalExplorer3.1* (Wolff *et al.*, 2012). In the FP plots, d_i and d_e are the distances from the Hirshfeld surface to the nearest atoms outside and inside the surface. The blue colour represents a low frequency of

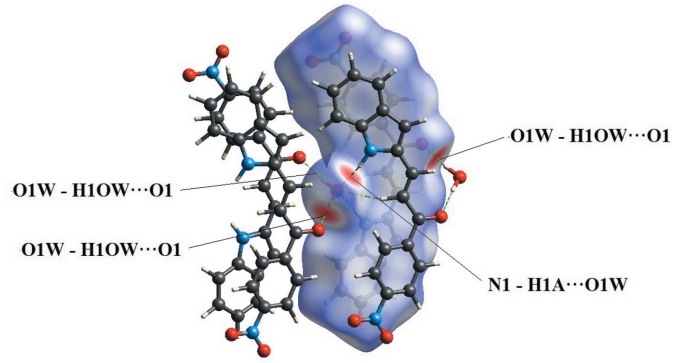

Figure 4
Hirshfeld surface of the title compound mapped over d_{norm}.

occurrence of a (d_i, d_e) pair and the full fingerprint is outlined in grey (Ternavisk *et al.*, 2014). The water molecule and H···O interactions are visualized as bright-red spots on the Hirshfeld surface mapped over d_{norm} with neighbouring molecules connected by O1*W*—H1*OW*···O1 and N1—H1*A*···O1 hydrogen bonds (Fig. 4). The fingerprint plots indicate the percentage contributions of the various intermolecular contacts (Fig. 5). The H···H contacts clearly make the most significant contribution (36.6%), whereas O···H/H···O and C···H/H···C contacts make contributions of 29.9 and 12.5%, respectively, to the Hirshfeld surface. The presence of O···H/H···O interactions is indicated by two symmetrical narrow spikes with $d_i + d_e$ ~1.7 Å arise specifically due to hydrogen-bonding interactions between the water H atom and the carbonyl oxygen. Furthermore, the existence of C···H/H···C interactions is shown by the pair of characteristics wings with the edge at $d_i + d_e$ ~2.9 Å, which is due to the contribution of C—H···π interaction. The 11.5% contribution of the C···C interactions arises from the π–π interaction, where the sum of d_i and d_e obtained is quite similar at 3.5 Å. Interestingly, the N···H contacts showed a 2.6% contribution elucidated by a butterfly fingerprint plot resulting from the N1—H1*A*···O1 interaction.

The presence of the C—H···π interactions can be seen in the pale-orange spot inside the circle of black arrows on the Hirshfeld surface mapped over d_e in (Fig. 6*a*). With the shape-

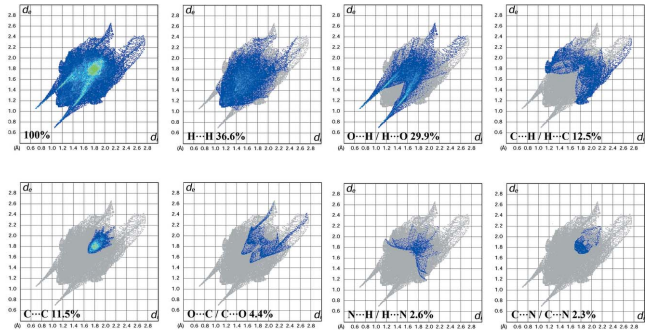

Figure 5
Fingerprint plots of the intermolecular interactions showing the percentage contributions to the total Hirshfeld surface.

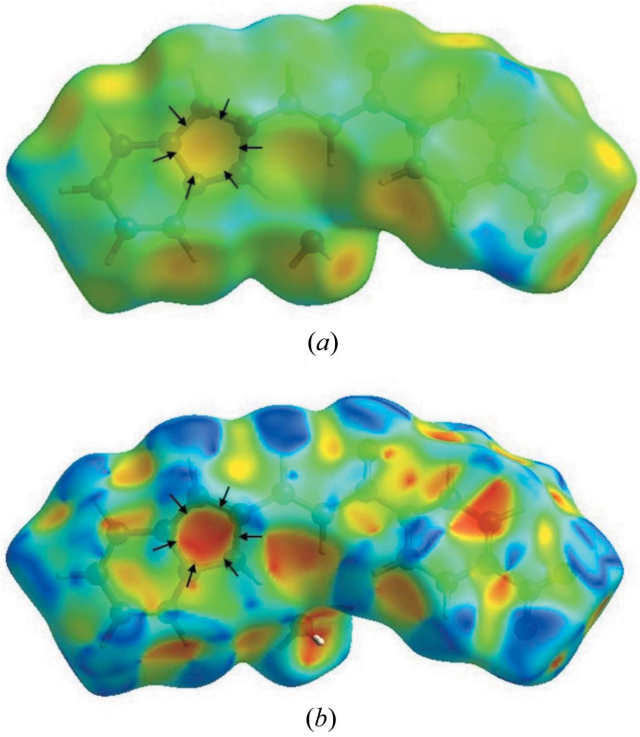

Figure 6
Graphical view of the Hirshfeld surfaces for the title compound (*a*) mapped over d_e with a pale-orange spot and (*b*) mapped over shape-index with a bright-red spot, both inside the black arrows, signifying the involvement of the C—H···π interactions.

indexed mapping, the C—H···π interactions can be observed as a bright-red spot identified with black arrows in Fig. 6*b*. The blue spots near the ring represent the reciprocal C—H···π interactions.

5. Frontier molecular orbital and UV–vis studies

Frontier molecular orbital analysis is a vital tool in the development of molecular electronic properties. The energy gap (E_g) between the highest occupied molecular orbital (HOMO) and lowest unoccupied molecular orbital (LUMO) is a crucial factor in elucidating the molecular electrical transport properties. In the present study, the HOMO and LUMO were computed at the DFT/B3LYP/6-311G++(d,p) theoretical level and the respective plots of the frontier molecular orbital are illustrated in Fig. 7. At a specific separation between donor and acceptor, charge transfer may occur in the ground state if the HOMO of the donor lies energetically above the LUMO of the acceptor (Caruso *et al.*, 2014). As can be seen from Fig. 7, the charge at the HOMO state is more localized at the indole group and enone moiety while charge is accumulated entirely at the nitro-substituted phenyl ring and the enone moiety in the LUMO state. The results reveal that the intramolecular charge transfer (ICT) occurred from the electron-donor groups to the electron-acceptor groups through the enone moiety. The carbon–carbon double bond connecting the donor and acceptor groups is responsible for the charge movement through π-conjugation, triggering electronic delocalization within the molecule (Prabhu *et al.*, 2015). The energy gap of 2.80 eV obtained from the DFT calculations indicates strong chemical reactivity and weaker kinetic stability, which increase the polarizability and NLO properties (Maidur *et al.*, 2018).

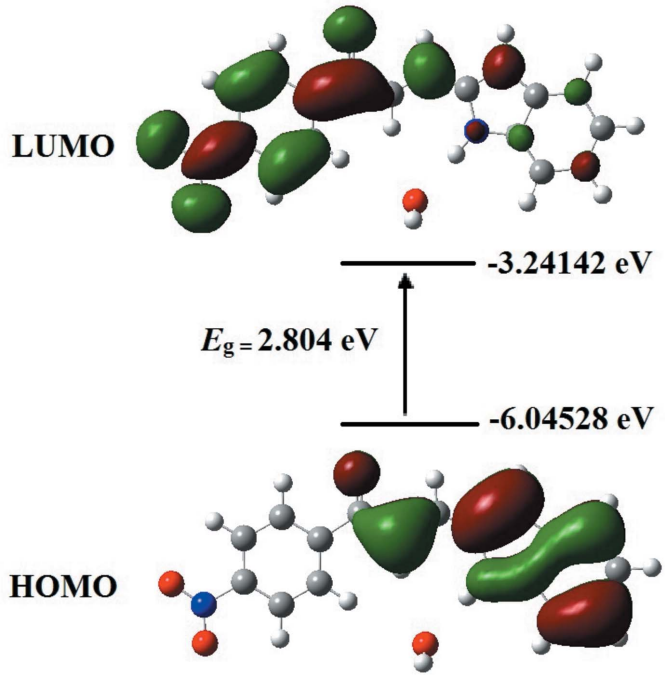

Figure 7
Molecular orbitals showing electronic transition between HOMO–LUMO of the title compound.

The absorption spectrum of the title compound was carried out in acetonitrile with a concentration of 10^{-4} *M*. The absorption spectrum comprises of four major bands (Fig. 8). The strongest band occurs in the region of 396 nm, which was assigned to π–π^* transition. This sharp peak is suspected to arise from the indole ring and carbonyl group (C═O). The second strong UV–vis band is observed at 269 nm and is mainly attributed to the electron-withdrawing substituent of

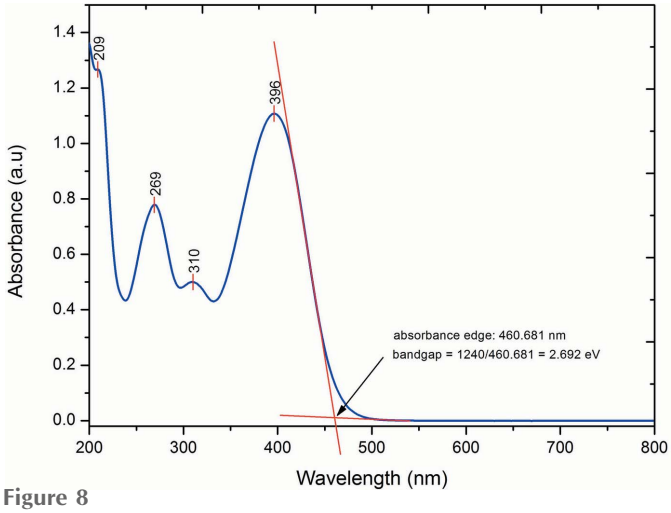

Figure 8
The UV–vis absorption spectrum of the title compound.

Table 2
Experimental details.

Crystal data	
Chemical formula	$2C_{17}H_{12}N_2O_3{\cdot}H_2O$
M_r	602.59
Crystal system, space group	Monoclinic, *C*2/*c*
Temperature (K)	296
a, *b*, *c* (Å)	14.835 (7), 6.453 (2), 28.000 (11)
β (°)	93.505 (10)
V (Å^3)	2675.4 (18)
Z	4
Radiation type	Mo $K\alpha$
μ (mm^{-1})	0.11
Crystal size (mm)	0.83 × 0.31 × 0.04
Data collection	
Diffractometer	Bruker APEXII CCD
Absorption correction	Multi-scan (*SADABS*; Bruker, 2009)
T_{min}, T_{max}	0.638, 0.955
No. of measured, independent and observed [$I > 2\sigma(I)$] reflections	36005, 2369, 1263
R_{int}	0.129
(sin $\theta/\lambda)_{max}$ (Å^{-1})	0.595
Refinement	
$R[F^2 > 2\sigma(F^2)]$, $wR(F^2)$, S	0.061, 0.190, 1.07
No. of reflections	2369
No. of parameters	213
H-atom treatment	H atoms treated by a mixture of independent and constrained refinement
$\Delta\rho_{max}$, $\Delta\rho_{min}$ (e Å^{-3})	0.22, −0.19

Computer programs: *APEX2* and *SAINT* (Bruker, 2009), *SHELXS97* (Sheldrick 2008), *SHELXL2013* (Sheldrick, 2015), *DIAMOND* (Brandenburg, 2009), *Mercury* (Macrae *et al.*, 2008) and *PLATON* (Spek, 2009).

the nitro group (Pavia *et al.*, 2001). The energy gap of the title compound was calculated from the UV–vis absorption edge at 461 nm (Fig. 8), giving an energy band gap value of 2.70 eV, comparable with the HOMO–LUMO energy gap obtained from the DFT study. This band gap is similar to those in reported studies (D'silva *et al.*, 2011) and within the energy-gap range for semiconducting materials (Emmanuel *et al.*, 2002).

6. Database survey

A search of the Cambridge Structural Database (Version 5.39, last update November 2017; Groom *et al.*, 2016) revealed closely related compounds that differ in the donor substituents: 1-(4-nitrophenyl)-3-(pyren-1-yl)prop-2-en-1-one (Yu *et al.*, 2017), 3-(2-furyl)-1-(4-nitrophenyl)prop-2-en-1-one) (Patil *et al.*, 2006) and 1-(4-nitrophenyl)-3-(2-thienyl)prop-2-en-1-one (Teh *et al.*, 2006) with pyrene, furan and thiophene donor substituent rings. Other related compounds include (2*E*)-3-(2-methylphenyl)-1-(4-nitrophenyl)prop-2-en-1-one (Prabhu *et al.*, 2015) and 3-(4-methoxyphenyl)-1-(4-nitrophenyl)prop-2-en-1-one (Patil *et al.*, 2006).

7. Synthesis and crystallization

The title compound was synthesized *via* a Claisen–Schmidt condensation reaction. A mixture of 1-(4-nitrophenyl)ethanone (0.5 mmol) and indole-2-carboxaldehyde (0.5 mmol) was dissolved in methanol (20 mL). Sodium hydroxide (NaOH) solution was then added dropwise under vigorous stirring. The reaction mixture was stirred for 5–6 h at room temperature. The final precipitate was filtered, washed with distilled water and recrystallized by slow evaporation from acetone solution to obtain orange plate-shaped crystals.

8. Refinement

Crystal data collection and structure refinement details are summarized in Table 2. All C-bound H atoms were positioned geometrically (C—H = 0.93 Å) and refined using a riding model with U_{iso}(H) = 1.2U_{eq}(C). The water O atom was refined with half-occupancy. The O- and N-bound H atoms were located from difference-Fourier maps and refined freely.

Funding information

The authors would like to thank the Malaysian Government and Universiti Sains Malaysia (USM) for providing facilities and funding to conduct this research under the Fundamental Research Grant Scheme (FRGS) No. 203.PFIZIK.6711572 and Short-Term No. 203.PFIZIK.6711606.

References

Brandenburg, K. B. M. (2009). *DIAMOND*. University of Bonn, Germany.
Bruker (2009). *APEX2*, *SAINT* and *SADABS*. Bruker AXS Inc., Madison, Wisconsin, USA.
Caruso, F., Atalla, V., Ren, X., Rubio, A., Scheffler, M. & Rinke, P. (2014). *Phys. Rev. B*, **90**, 085141.
Dobrowolski, M. A., Krygowski, T. M. & Cyranski, M. K. (2009). *Croat. Chem. Acta*, **82**, 139–147.
D'silva, E. D., Podagatlapalli, G. K., Rao, S. V., Rao, D. N. & Dharmaprakash, S. M. (2011). *Cryst. Growth Des.* **11**, 5362–5369.
Emmanuel, R. & Borge, V. (2002). *In Optoelectronics*. New York: Cambridge University, Press.
Groom, C. R., Bruno, I. J., Lightfoot, M. P. & Ward, S. C. (2016). *Acta Cryst*. B**72**, 171–179.
Kozlowski, D., Trouillas, P., Calliste, C., Marsal, P., Lazzaroni, R. & Duroux, J.-L. (2007). *J. Phys. Chem. A*, **111**, 1138–1145.
Macrae, C. F., Bruno, I. J., Chisholm, J. A., Edgington, P. R., McCabe, P., Pidcock, E., Rodriguez-Monge, L., Taylor, R., van de Streek, J. & Wood, P. A. (2008). *J. Appl. Cryst.* **41**, 466–470.
Maidur, S. R., Jahagirdar, J. R., Patil, P. S., Chia, T. S. & Quah, C. K. (2018). *Opt. Mater.* **75**, 580–594.
Patil, P. S., Teh, J. B.-J., Fun, H.-K., Razak, I. A. & Dharmaprakash, S. M. (2006). *Acta Cryst.* E**62**, o2397–o2398.
Pavia, D. L., Lampman, G. M. & Kriz, G. S. (2001). *Introduction to Spectroscopy*, 3rd ed, pp. 378–379. Australia: Brooks/Cole-Thomson Learning.
Prabhu, S. R., Jayarama, A., Upadhyaya, V., Bhat, K. S. & Ng, S. W. (2015). *Mol. Cryst. Liq. Cryst.* **607**, 200–214.
Sheldrick, G. M. (2008). *Acta Cryst.* A**64**, 112–122.
Sheldrick, G. M. (2015). *Acta Cryst.* C**71**, 3–8.
Spek, A. L. (2009). *Acta Cryst.* D**65**, 148–155.
Teh, J. B.-J., Patil, P. S., Fun, H.-K., Razak, I. A. & Dharmaprakash, S. M. (2006). *Acta Cryst.* E**62**, o3957–o3958.
Ternavisk, R. R., Camargo, A. J., Machado, F. B. C., Rocco, J. A. F. F., Aquino, G. L. B., Silva, V. H. C. & Napolitano, H. B. (2014). *J. Mol. Model.* **20**, 2526–2536.

Thanigaimani, K., Arshad, S., Khalib, N. C., Razak, I. A., Arunagiri, C., Subashini, A., Sulaiman, S. F., Hashim, N. S. & Ooi, K. L. (2015). *Spectrochim. Acta A*, **149**, 90–102.
Toledo, T. A. de, da Costa, R. C., Bento, R. R. F., Al-Maqtari, H. M., Jamalis, J. & Pizani, P. S. (2018). *J. Mol. Struct.* **1155**, 634–645.
Wolff, S. K., Grimwood, D. J., McKinnon, J. J., Turner, M. J., Jayatilaka, D. & Spackman, M. A. (2012). *Crystal Explorer.* University of Western Australia, Perth.
Yu, F., Wang, M., Sun, H., Shan, Y., Du, M., Khan, A., Usman, R., Zhang, W., Shan, H. & Xu, C. (2017). *RSC Adv.* **7**, 8491–8503.
Zainuri, D. A., Arshad, S., Khalib, N. C., Razak, A. I., Pillai, R. R., Sulaiman, F., Hashim, N. S., Ooi, K. L., Armaković, S., Armaković, S. J., Panicker, Y. & Van Alsenoy, C. (2017). *J. Mol. Struct.* **1128**, 520–533.
Zheng, Y.-Z., Zhou, Y., Liang, Q., Chen, D.-F., Guo, R. & Lai, R. C. (2016). *Sci. Rep.* **6**, 34647.

supporting information

Acta Cryst. (2018). E**74**, 1589-1594 [https://doi.org/10.1107/S2056989018014329]

Crystal structure and optical spectroscopic analyses of (*E*)-3-(1*H*-indol-2-yl)-1-(4-nitrophenyl)prop-2-en-1-one hemihydrate

Muhamad Fikri Zaini, Ibrahim Abdul Razak, Wan Mohd Khairul and Suhana Arshad

Computing details

Data collection: *APEX2* (Bruker, 2009); cell refinement: *SAINT* (Bruker, 2009); data reduction: *SAINT* (Bruker, 2009); program(s) used to solve structure: *SHELXS97* (Sheldrick 2008); program(s) used to refine structure: *SHELXL2013* (Sheldrick, 2015); molecular graphics: *DIAMOND* (Brandenburg, 2009) and *Mercury* (Macrae *et al.*, 2008); software used to prepare material for publication: *PLATON* (Spek, 2009).

(*E*)-3-(1*H*-indol-2-yl)-1-(4-nitrophenyl)prop-2-en-1-one hemihydrate

Crystal data

$2C_{17}H_{12}N_2O_3·H_2O$
M_r = 602.59
Monoclinic, *C*2/*c*
a = 14.835 (7) Å
b = 6.453 (2) Å
c = 28.000 (11) Å
β = 93.505 (10)°
V = 2675.4 (18) Å^3
Z = 4
F(000) = 1256
D_x = 1.496 Mg m^{-3}
Mo *Kα* radiation, *λ* = 0.71073 Å
Cell parameters from 1566 reflections
θ = 2.9–19.5°
μ = 0.11 mm^{-1}
T = 296 K
Plate, orange
0.83 × 0.31 × 0.04 mm

Data collection

Bruker APEXII CCD diffractometer
φ and *ω* scans
Absorption correction: multi-scan (SADABS; Bruker, 2009)
T_{min} = 0.638, T_{max} = 0.955
36005 measured reflections
2369 independent reflections
1263 reflections with $I > 2\sigma(I)$
R_{int} = 0.129
θ_{max} = 25.0°, θ_{min} = 2.8°
h = −17→17
k = −7→7
l = −33→33

Refinement

Refinement on F^2
Least-squares matrix: full
$R[F^2 > 2\sigma(F^2)]$ = 0.061
$wR(F^2)$ = 0.190
S = 1.07
2369 reflections
213 parameters
0 restraints
Hydrogen site location: mixed
H atoms treated by a mixture of independent and constrained refinement
$w = 1/[\sigma^2(F_o^2) + (0.0548P)^2 + 3.4801P]$ where $P = (F_o^2 + 2F_c^2)/3$
$(\Delta/\sigma)_{max} < 0.001$
$\Delta\rho_{max}$ = 0.22 e Å^{-3}
$\Delta\rho_{min}$ = −0.19 e Å^{-3}
Extinction correction: SHELXL, $Fc^*=kFc[1+0.001xFc^2\lambda^3/\sin(2\theta)]^{-1/4}$
Extinction coefficient: 0.0010 (4)

Special details

Experimental. The following wavelength and cell were deduced by SADABS from the direction cosines etc. They are given here for emergency use only: CELL 0.71150 6.604 8.276 28.665 93.349 89.966 113.537

Geometry. All esds (except the esd in the dihedral angle between two l.s. planes) are estimated using the full covariance matrix. The cell esds are taken into account individually in the estimation of esds in distances, angles and torsion angles; correlations between esds in cell parameters are only used when they are defined by crystal symmetry. An approximate (isotropic) treatment of cell esds is used for estimating esds involving l.s. planes.

Fractional atomic coordinates and isotropic or equivalent isotropic displacement parameters (Å²)

	x	*y*	*z*	U_{iso}*/U_{eq}
N1	0.8500 (2)	0.5670 (5)	0.21045 (11)	0.0608 (8)
H1A	0.892 (2)	0.494 (6)	0.2257 (13)	0.071 (12)*
N2	1.1251 (3)	0.4606 (7)	0.48886 (12)	0.0826 (11)
O1	0.98111 (17)	1.0824 (4)	0.33010 (9)	0.0713 (8)
O2	1.1071 (3)	0.2810 (6)	0.49214 (12)	0.1143 (13)
O3	1.1754 (2)	0.5484 (6)	0.51669 (11)	0.1137 (12)
C1	0.8028 (2)	0.5110 (6)	0.16995 (12)	0.0579 (9)
C2	0.8031 (3)	0.3301 (6)	0.14546 (14)	0.0712 (11)
H2A	0.8396	0.2200	0.1559	0.085*
C3	0.7485 (3)	0.3159 (7)	0.10529 (15)	0.0802 (12)
H3A	0.7470	0.1935	0.0877	0.096*
C4	0.6954 (3)	0.4782 (8)	0.09007 (15)	0.0802 (12)
H4A	0.6584	0.4637	0.0622	0.096*
C5	0.6950 (3)	0.6569 (7)	0.11385 (14)	0.0750 (12)
H5A	0.6590	0.7666	0.1025	0.090*
C6	0.7487 (2)	0.6766 (6)	0.15553 (13)	0.0620 (10)
C7	0.7659 (2)	0.8323 (6)	0.18888 (13)	0.0613 (10)
H7A	0.7388	0.9623	0.1884	0.074*
C8	0.8281 (2)	0.7644 (6)	0.22200 (12)	0.0569 (9)
C9	0.8692 (2)	0.8667 (6)	0.26162 (12)	0.0586 (10)
H9A	0.8545	1.0055	0.2656	0.070*
C10	0.9266 (2)	0.7848 (6)	0.29370 (12)	0.0603 (10)
H10A	0.9386	0.6439	0.2913	0.072*
C11	0.9717 (2)	0.8965 (6)	0.33203 (12)	0.0574 (9)
C12	1.0089 (2)	0.7823 (5)	0.37368 (12)	0.0560 (9)
C13	0.9864 (3)	0.5825 (6)	0.38163 (13)	0.0678 (11)
H13A	0.9450	0.5162	0.3605	0.081*
C14	1.0231 (3)	0.4790 (6)	0.41952 (13)	0.0694 (11)
H14A	1.0072	0.3421	0.4249	0.083*
C15	1.0831 (2)	0.5757 (6)	0.44943 (12)	0.0634 (10)
C16	1.1064 (3)	0.7740 (7)	0.44334 (14)	0.0729 (11)
H16A	1.1475	0.8391	0.4648	0.088*
C17	1.0683 (3)	0.8770 (6)	0.40510 (13)	0.0668 (11)
H17A	1.0832	1.0152	0.4004	0.080*
O1W	1.0000	0.3138 (6)	0.2500	0.0710 (11)
H1OW	1.012 (3)	0.237 (6)	0.2254 (14)	0.094 (15)*

Atomic displacement parameters (Å²)

	U^{11}	U^{22}	U^{33}	U^{12}	U^{13}	U^{23}
N1	0.061 (2)	0.063 (2)	0.0561 (19)	0.0041 (17)	−0.0096 (16)	0.0024 (16)
N2	0.090 (3)	0.093 (3)	0.063 (2)	0.004 (2)	−0.010 (2)	0.008 (2)
O1	0.0864 (19)	0.0584 (17)	0.0674 (17)	−0.0039 (14)	−0.0090 (14)	0.0005 (13)
O2	0.153 (3)	0.089 (2)	0.096 (2)	−0.002 (2)	−0.032 (2)	0.025 (2)
O3	0.128 (3)	0.128 (3)	0.079 (2)	−0.006 (2)	−0.043 (2)	0.007 (2)
C1	0.056 (2)	0.064 (2)	0.053 (2)	−0.0047 (18)	−0.0023 (17)	0.0009 (19)
C2	0.079 (3)	0.064 (3)	0.069 (3)	−0.002 (2)	−0.001 (2)	−0.008 (2)
C3	0.081 (3)	0.084 (3)	0.076 (3)	−0.014 (3)	0.006 (2)	−0.018 (2)
C4	0.065 (3)	0.106 (3)	0.068 (3)	−0.011 (3)	−0.008 (2)	−0.015 (3)
C5	0.067 (3)	0.087 (3)	0.069 (3)	0.004 (2)	−0.014 (2)	−0.003 (2)
C6	0.057 (2)	0.067 (2)	0.060 (2)	−0.004 (2)	−0.0039 (18)	0.002 (2)
C7	0.061 (2)	0.056 (2)	0.066 (2)	0.0046 (18)	−0.0078 (19)	0.005 (2)
C8	0.057 (2)	0.056 (2)	0.057 (2)	−0.0013 (18)	−0.0010 (18)	−0.0047 (18)
C9	0.057 (2)	0.060 (2)	0.058 (2)	−0.0015 (17)	−0.0025 (18)	−0.0025 (18)
C10	0.065 (2)	0.056 (2)	0.059 (2)	0.0033 (18)	−0.0023 (19)	−0.0037 (19)
C11	0.055 (2)	0.058 (2)	0.058 (2)	0.0012 (18)	−0.0013 (18)	−0.0020 (19)
C12	0.056 (2)	0.055 (2)	0.056 (2)	0.0008 (18)	−0.0019 (18)	−0.0055 (18)
C13	0.072 (3)	0.065 (2)	0.064 (2)	−0.008 (2)	−0.015 (2)	0.002 (2)
C14	0.077 (3)	0.065 (3)	0.064 (2)	−0.006 (2)	−0.006 (2)	0.002 (2)
C15	0.068 (2)	0.070 (3)	0.051 (2)	0.004 (2)	−0.0066 (19)	0.000 (2)
C16	0.079 (3)	0.076 (3)	0.062 (2)	−0.010 (2)	−0.012 (2)	−0.007 (2)
C17	0.072 (2)	0.064 (2)	0.063 (2)	−0.008 (2)	−0.010 (2)	−0.005 (2)
O1W	0.091 (3)	0.055 (2)	0.065 (3)	0.000	−0.012 (2)	0.000

Geometric parameters (Å, º)

N1—C1	1.345 (4)	C7—H7A	0.9300
N1—C8	1.359 (4)	C8—C9	1.399 (5)
N1—H1A	0.87 (4)	C9—C10	1.310 (5)
N2—O3	1.189 (4)	C9—H9A	0.9300
N2—O2	1.194 (4)	C10—C11	1.426 (5)
N2—C15	1.440 (5)	C10—H10A	0.9300
O1—C11	1.209 (4)	C11—C12	1.459 (5)
C1—C2	1.354 (5)	C12—C17	1.353 (5)
C1—C6	1.382 (5)	C12—C13	1.353 (5)
C2—C3	1.348 (5)	C13—C14	1.341 (5)
C2—H2A	0.9300	C13—H13A	0.9300
C3—C4	1.363 (6)	C14—C15	1.338 (5)
C3—H3A	0.9300	C14—H14A	0.9300
C4—C5	1.332 (5)	C15—C16	1.339 (5)
C4—H4A	0.9300	C16—C17	1.354 (5)
C5—C6	1.378 (5)	C16—H16A	0.9300
C5—H5A	0.9300	C17—H17A	0.9300
C6—C7	1.385 (5)	O1W—H1OW	0.88 (4)
C7—C8	1.341 (4)		

C1—N1—C8	109.4 (3)	N1—C8—C9	122.2 (3)
C1—N1—H1A	126 (2)	C10—C9—C8	126.0 (4)
C8—N1—H1A	124 (2)	C10—C9—H9A	117.0
O3—N2—O2	123.1 (4)	C8—C9—H9A	117.0
O3—N2—C15	118.8 (4)	C9—C10—C11	124.6 (3)
O2—N2—C15	118.1 (4)	C9—C10—H10A	117.7
N1—C1—C2	129.9 (4)	C11—C10—H10A	117.7
N1—C1—C6	107.6 (3)	O1—C11—C10	121.2 (3)
C2—C1—C6	122.6 (3)	O1—C11—C12	119.9 (3)
C3—C2—C1	117.4 (4)	C10—C11—C12	118.9 (3)
C3—C2—H2A	121.3	C17—C12—C13	118.7 (4)
C1—C2—H2A	121.3	C17—C12—C11	119.4 (3)
C2—C3—C4	121.0 (4)	C13—C12—C11	121.9 (3)
C2—C3—H3A	119.5	C14—C13—C12	120.8 (4)
C4—C3—H3A	119.5	C14—C13—H13A	119.6
C5—C4—C3	122.0 (4)	C12—C13—H13A	119.6
C5—C4—H4A	119.0	C15—C14—C13	119.0 (4)
C3—C4—H4A	119.0	C15—C14—H14A	120.5
C4—C5—C6	118.9 (4)	C13—C14—H14A	120.5
C4—C5—H5A	120.6	C14—C15—C16	122.2 (4)
C6—C5—H5A	120.6	C14—C15—N2	118.6 (4)
C5—C6—C1	118.1 (4)	C16—C15—N2	119.2 (4)
C5—C6—C7	135.3 (4)	C15—C16—C17	118.2 (4)
C1—C6—C7	106.5 (3)	C15—C16—H16A	120.9
C8—C7—C6	108.6 (3)	C17—C16—H16A	120.9
C8—C7—H7A	125.7	C12—C17—C16	121.0 (4)
C6—C7—H7A	125.7	C12—C17—H17A	119.5
C7—C8—N1	107.8 (3)	C16—C17—H17A	119.5
C7—C8—C9	130.0 (4)		

C8—N1—C1—C2	179.9 (4)	C8—C9—C10—C11	175.8 (3)
C8—N1—C1—C6	−0.6 (4)	C9—C10—C11—O1	−21.9 (6)
N1—C1—C2—C3	−179.9 (4)	C9—C10—C11—C12	159.5 (4)
C6—C1—C2—C3	0.6 (6)	O1—C11—C12—C17	−13.1 (5)
C1—C2—C3—C4	0.2 (6)	C10—C11—C12—C17	165.5 (3)
C2—C3—C4—C5	0.0 (7)	O1—C11—C12—C13	167.7 (4)
C3—C4—C5—C6	−1.2 (6)	C10—C11—C12—C13	−13.7 (5)
C4—C5—C6—C1	1.9 (6)	C17—C12—C13—C14	−0.9 (6)
C4—C5—C6—C7	179.8 (4)	C11—C12—C13—C14	178.3 (4)
N1—C1—C6—C5	178.7 (3)	C12—C13—C14—C15	−0.4 (6)
C2—C1—C6—C5	−1.7 (6)	C13—C14—C15—C16	1.3 (6)
N1—C1—C6—C7	0.2 (4)	C13—C14—C15—N2	−177.3 (4)
C2—C1—C6—C7	179.8 (3)	O3—N2—C15—C14	−176.8 (4)
C5—C6—C7—C8	−177.8 (4)	O2—N2—C15—C14	2.8 (6)
C1—C6—C7—C8	0.3 (4)	O3—N2—C15—C16	4.5 (6)
C6—C7—C8—N1	−0.6 (4)	O2—N2—C15—C16	−176.0 (4)
C6—C7—C8—C9	177.6 (4)	C14—C15—C16—C17	−0.9 (6)

C1—N1—C8—C7	0.7 (4)	N2—C15—C16—C17	177.8 (4)
C1—N1—C8—C9	−177.7 (3)	C13—C12—C17—C16	1.4 (6)
C7—C8—C9—C10	176.4 (4)	C11—C12—C17—C16	−177.9 (4)
N1—C8—C9—C10	−5.5 (6)	C15—C16—C17—C12	−0.5 (6)

Hydrogen-bond geometry (Å, º)

Cg1 is the centroid of the N1/C1/C6–C8 ring.

D—H···*A*	*D*—H	H···*A*	*D*···*A*	*D*—H···*A*
O1*W*—H1*OW*···O1^{i}	0.88 (4)	1.86 (4)	2.723 (4)	171 (4)
N1—H1*A*···O1*W*	0.87 (3)	2.06 (3)	2.923 (4)	170 (3)
C4—H4*A*···O2^{ii}	0.93	2.60	3.405 (6)	146
C9—H9*A*···*Cg*1^{iii}	0.93	2.87	3.518 (4)	127

Symmetry codes: (i) −*x*+2, *y*−1, −*z*+1/2; (ii) *x*−1/2, −*y*+1/2, *z*−1/2; (iii) −*x*+3/2, *y*+1/2, −*z*+1/2.